Supercooled spin liquid state in the frustrated pyrochlore $Dy_2Ti_2O_7$

Ethan R. Kassner[a], Azar B. Eyvazov[a], Benjamin Pichler[a,b], Timothy J. S. Munsie[c,d], Hanna A. Dabkowska[c], Graeme M. Luke[c,d,e], and J. C. Séamus Davis[a,f,g,h,1]

[a]Laboratory of Atomic and Solid State Physics, Department of Physics, Cornell University, Ithaca, NY 14853; [b]Department of Physics, Stanford University, Palo Alto, CA 94301; [c]Brockhouse Institute for Materials Research, McMaster University, Hamilton, ON, Canada, L8S 4L8; [d]Department of Physics, McMaster University, Hamilton, ON, Canada, L8S 4M1; [e]Canadian Institute for Advanced Research, Toronto, ON, Canada M5G 1Z8; [f]Condensed Matter Physics and Materials Science Department, Brookhaven National Laboratory, Upton, NY 11973; [g]School of Physics, University of St. Andrews, St. Andrews, Fife KY16 9SS, United Kingdom; and [h]Kavli Institute at Cornell for Nanoscale Science, Cornell University, Ithaca, NY 14850

Contributed by J. C. Séamus Davis, June 8, 2015 (sent for review April 10, 2015; reviewed by Zohar Nussinov and Peter Schiffer)

A "supercooled" liquid develops when a fluid does not crystallize upon cooling below its ordering temperature. Instead, the microscopic relaxation times diverge so rapidly that, upon further cooling, equilibration eventually becomes impossible and glass formation occurs. Classic supercooled liquids exhibit specific identifiers including microscopic relaxation times diverging on a Vogel–Tammann–Fulcher (VTF) trajectory, a Havriliak–Negami (HN) form for the dielectric function $\varepsilon(\omega, T)$, and a general Kohlrausch–Williams–Watts (KWW) form for time-domain relaxation. Recently, the pyrochlore $Dy_2Ti_2O_7$ has become of interest because its frustrated magnetic interactions may, in theory, lead to highly exotic magnetic fluids. However, its true magnetic state at low temperatures has proven very difficult to identify unambiguously. Here, we introduce high-precision, boundary-free magnetization transport techniques based upon toroidal geometries and gain an improved understanding of the time- and frequency-dependent magnetization dynamics of $Dy_2Ti_2O_7$. We demonstrate a virtually universal HN form for the magnetic susceptibility $\chi(\omega, T)$, a general KWW form for the real-time magnetic relaxation, and a divergence of the microscopic magnetic relaxation rates with the VTF trajectory. Low-temperature $Dy_2Ti_2O_7$ therefore exhibits the characteristics of a supercooled magnetic liquid. One implication is that this translationally invariant lattice of strongly correlated spins may be evolving toward an unprecedented magnetic glass state, perhaps due to many-body localization of spin.

spin liquid | supercooled liquids | magnetic dynamics | periodic boundaries

Cooling a pure liquid usually results in crystallization via a first-order phase transition. However, in glass-forming liquids when the cooling is sufficiently rapid, a metastable "supercooled" state is achieved instead (1–3). Here, the microscopic relaxation times diverge until equilibration of the system is no longer possible at a given cooling rate. At this juncture there is generally a broad peak in the specific heat preceding the glass transition, at which no symmetry-breaking phase transition occurs (Fig. 1*A*). The antecedent fluid exhibits a set of phenomena characteristic of the supercooled liquid state (1–3). For example, the divergence of microscopic relaxation times $\tau_0(T)$ typically shows substantial departures from Arrhenius behavior $[\tau_0(T) = A\exp(\Delta/kT)]$ and, instead, is described characteristically using the Vogel–Tammann–Fulcher (VTF) form (4)

$$\tau_0(T) = A\exp\left(\frac{DT_0}{T - T_0}\right). \quad [1]$$

Here, T_0 is a temperature at which the relaxation time diverges to ∞ while D characterizes the extent of the super-Arrhenius behavior (Fig. 1*B*). One way to establish $\tau_0(T)$ is by measuring the characteristic frequency $\omega_0(T) = 1/\tau_0(T)$ of peaks in the dissipative (imaginary) component of the dielectric function $\varepsilon(\omega, T)$. For classic supercooled liquids, $\varepsilon(\omega, T)$ generally exhibits the Havriliak–Negami (HN) form (5, 6)

$$\varepsilon(\omega, T) = \varepsilon_\infty + \frac{\varepsilon_0}{(1 + (i\omega\tau_{HN})^\alpha)^\gamma}. \quad [2]$$

Here, the exponents α and γ describe, respectively, the broadening and asymmetry of the relaxation in frequency compared with a simple Debye form ($\alpha = \gamma = 1$), $\tau_{HN}(T)$ is the microscopic relaxation time, and ϵ_∞ is a purely real quantity that describes the relaxation in the $\omega \to \infty$ limit. The HN forms of $\mathrm{Re}[\varepsilon(\omega, T)]$ and $\mathrm{Im}[\varepsilon(\omega, T)]$ that are characteristic of supercooled liquids are shown in Fig. 1*C*. In the time domain, this relaxation is described by the classic Kohlrausch–Williams–Watts (KWW) form (7)

$$\varepsilon(t) = \varepsilon_0\exp\left[-\left(\frac{t}{\tau_{KWW}}\right)^\beta\right], \quad [3]$$

where $\varepsilon(t)$ describes the evolution of polarization $\boldsymbol{P}(\mathrm{t})$, τ_{KWW} is the microscopic relaxation time, and $0 < \beta < 1$ is a "stretching exponent" (Fig. 1*D*). Debye relaxation corresponds to $\beta = 1$ whereas $\beta < 1$ typically indicates the presence of a more complex energy barrier distribution. Although the KWW function has no analytic Fourier transform when $\beta \neq 1/2$, KWW and HN are

Significance

Frustrated magnetic pyrochlore systems, in which there are many possible favored spin configurations, may host a variety of exotic magnetic phases. For example, some models predict that $Dy_2Ti_2O_7$ hosts a fluid of mobile magnetic "monopoles" that interact via a magnetic Coulomb interaction. Here, we introduce a novel measurement technique that realizes periodic boundary conditions, and use it to examine the magnetization transport dynamics of tori of $Dy_2Ti_2O_7$. We identify multiple phenomena in the dynamics of $Dy_2Ti_2O_7$ that are characteristic of a supercooled magnetic liquid approaching a glass transition. This highly unusual classical spin liquid forms in a structurally ordered crystal and therefore it may constitute the approach to a novel magnetic glass state.

Author contributions: E.R.K. and J.C.S.D. designed research; E.R.K., A.B.E., and B.P. performed research; E.R.K. and A.B.E. analyzed data; T.J.S.M. and H.A.D. synthesized the samples; G.M.L. supervised the research and synthesized samples; J.C.S.D. supervised the research; and E.R.K., A.B.E., G.M.L., and J.C.S.D. wrote the paper.

Reviewers: Z.N., Washington University in St. Louis; and P.S., University of Illinois at Urbana–Champaign.

The authors declare no conflict of interest.

Freely available online through the PNAS open access option.

[1]To whom correspondence should be addressed. Email: jcseamusdavis@gmail.com.

This article contains supporting information online at www.pnas.org/lookup/suppl/doi:10.1073/pnas.1511006112/-/DCSupplemental.

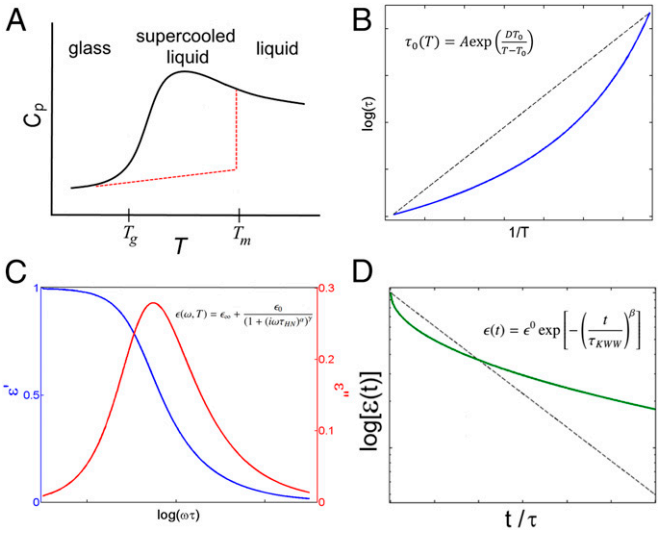

Fig. 1. Signatures of supercooling in classic glass-forming fluids. (*A*) Under suitable conditions, a liquid can be cooled through the melting temperature T_m without crystallizing and instead reaches a supercooled liquid state. With further cooling, the heat capacity of the supercooled liquid must eventually decrease from the higher liquid value toward the lower crystalline value; this is necessary for the entropy to remain nonnegative at very low temperatures. Supercooled liquids therefore typically have a broad peak in their heat capacity below T_m and a little above the glass transition temperature T_g. (*B*) In a classic supercooled liquid, diverging microscopic relaxation times $\tau_0(T)$ typically do not follow Arrhenius behavior (dashed line) but instead follow the VTF evolution (blue curve; Eq. **1**). Here, T_0 is a temperature at which the relaxation time diverges to ∞ while *D* characterizes the extent of the super-Arrhenius behavior. By convention, a classic glass is said to form when $\tau_0 > 100$ s. (*C*) Re$[\varepsilon(\omega, T)]$ and Im$[\varepsilon(\omega, T)]$ of the HN form (Eq. **2**) of the dielectric function; these are both characteristic of supercooled liquids. (*D*) Ultraslow relaxation in glass-forming liquids occurs with a KWW form (green curve, Eq. **3**) instead of a Debye form (dashed line), as shown here for the dielectric function $\varepsilon(t)$.

actually complementary descriptions of the same microscopic phenomena, being connected by the relations (8)

$$\ln\left(\frac{\tau_{HN}}{\tau_{KWW}}\right) = 2.6(1-\beta)^{0.5}\exp(-3\beta) \text{ with } \alpha\gamma = \beta^{1.23}. \quad [4]$$

Observation of this HN/KWW phenomenology is the generally used standard by which classic supercooled fluids are identified (1–4).

Magnetization Dynamics Studies of $Dy_2Ti_2O_7$

Frustrated magnetic pyrochlores are now the focus of widespread interest because of the possibility that they can support different exotic magnetic phases (9–14). The pyrochlore $Dy_2Ti_2O_7$ is one of the most widely studied; it consists of highly magnetic Dy^{3+} ions in a sublattice comprising corner-sharing tetrahedra (Fig. 2*A*), and an interpenetrating octahedral lattice of Ti^{4+} and O^{2-} ions playing no magnetic role. Crystal fields break the angular-momentum-state degeneracy and cause the Dy^{3+} moments ($J = 15/2$, $\mu \approx 10\mu_B$) to point along their local [111] directions (15). Although high-temperature susceptibility measurements indicate a Curie–Weiss temperature of ∼1.2 K (16), both low-temperature susceptibility (16) and muon spin-rotation studies (17) have revealed no magnetic ordering transition in $Dy_2Ti_2O_7$ down to $T \sim 50$ mK. Additionally, a broad peak in the specific heat (18–22) centered around $T \approx 1.0$ K occurs at or below the transition temperature that might be expected from the Curie–Weiss temperature, but no phase transition occurs. By contrast, in a typical paramagnet the heat capacity would exhibit a sharp peak at the ordering temperature below which long-range magnetic order would become apparent in, for example, magnetic susceptibility, muon spin rotation, and neutron scattering; none of these ordering indications are observed in $Dy_2Ti_2O_7$. Instead, dipole and exchange interactions combine to create an effective nearest-neighbor Ising interaction of the form $-J_{eff}\sum \boldsymbol{S}_i \cdot \boldsymbol{S}_j$ with $J_{eff} \approx 1.1$ K (23). A consequence of this interaction in the pyrochlore geometry is that there are six possible equivalent magnetic ground-state conformations of a single $Dy_2Ti_2O_7$ tetrahedron; these can be mapped to the Bernal–Fowler ("2-in, 2-out") rules that govern hydrogen bond configurations in water ice but now it is a 2-in, 2-out arrangement of Dy^{3+} moments (Fig. 2*B*). This elegant "spin-ice" configuration has been firmly established (10, 14, 21, 22, 24). Theoretically, the long-range dipole interactions can also generate magnetic ordering (10, 14, 25) but, significantly, this has not been observed down to temperatures below 50 mK.

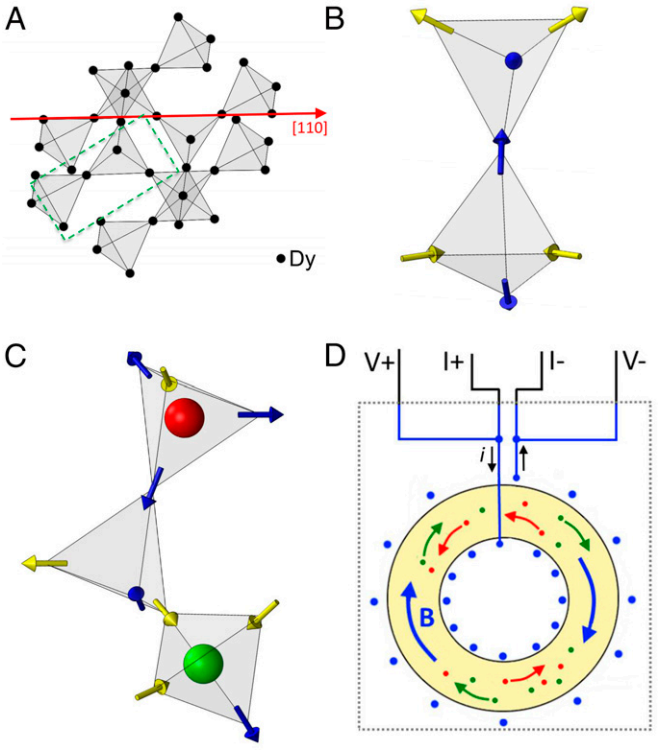

Fig. 2. Novel experimental techniques for frustrated magnetism in $Dy_2Ti_2O_7$. (*A*) The Dy^{3+} moments (black circles) in $Dy_2Ti_2O_7$ are located on a lattice comprising equilateral corner-sharing tetrahedra. The centers of tetrahedra themselves form a diamond lattice. (*B*) An allowed magnetic ground-state configuration for two tetrahedra in $Dy_2T_2iO_7$. Here, the crystal field anisotropy causes the moments to point along their local [111] axes, thus forcing them to point toward or away from each tetrahedron center. To minimize magnetic energy, the spin configurations of a tetrahedron of $Dy_2T_2iO_7$ satisfy the spin equivalent of the Bernal–Fowler "ice rules," with each tetrahedron having two spins pointing toward its center and two spins pointing away from its center. (*C*) Schematic of a pair of delocalized magnetic monopoles (green, red). (*D*) Schematic representation of the toroidal geometry of our $Dy_2Ti_2O_7$ sample (yellow) and the superconducting toroidal solenoid (blue). The cryogenic sample environment 30 mK < *T* < 4 K is indicated by a dashed rectangle. dc current flow in the direction indicated by black arrow produces an azimuthal static magnetic field *B* (blue arrows). If a fluid of delocalized magnetic monopoles of both signs exists, the net magnetization current $J\phi$ (red/green arrows) would be nonzero. Applied ac currents $I_0\cos(\omega t)$ generate the azimuthal fields $H\phi\cos(\omega t)$ whose effect is simultaneously detected by measuring the EMF across the STS: $V(\omega, T)$. The dynamical magnetic susceptibility components are then derived from $V_x(\omega, T) = -I_0\omega L\chi''$, $V_y(\omega, T) = -I_0\omega L\chi'$, where *L* is the effective geometrical inductance of the STS.

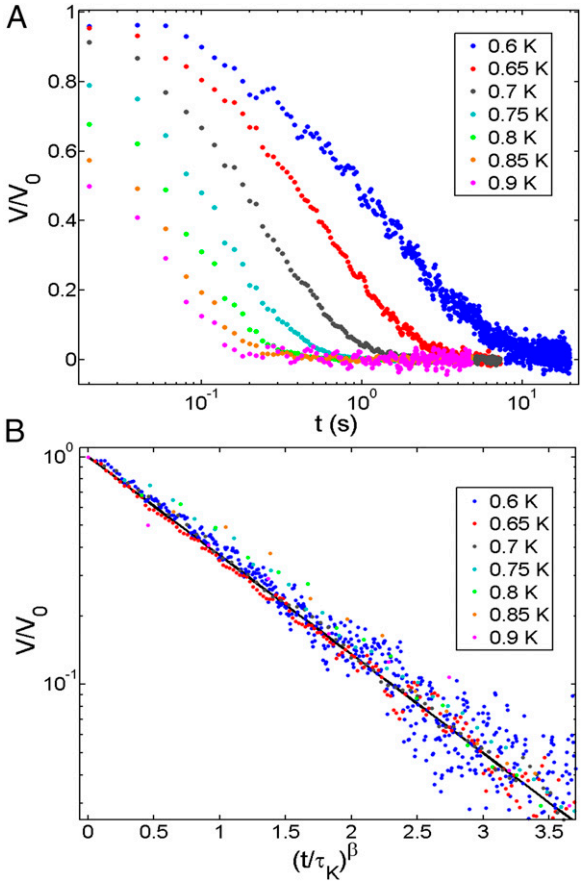

Fig. 3. KWW magnetization transient dynamics. (*A*) Typical examples of measured $V(t,T)$ of $Dy_2Ti_2O_7$ torus after the current is switched off in the STS. (*B*) The KWW collapse of all measured $V(t,T)$ transients from our $Dy_2Ti_2O_7$ torus experiments at the temperatures shown. Data at all temperatures collapse onto a simple exponential curve $V(x) = \exp(-x)$ (black line) when plotted using scaled KWW time parameters $x(t)$ as defined in the text. Clearly, a KWW relaxation model provides an excellent description of the data over the entire range of temperatures at which the d***M***/dt signals are resolvable.

The magnetic excited states of $Dy_2Ti_2O_7$ are then of great interest. One conjecture is that the magnetization dynamics may be described as a fluid of emergent delocalized magnetic monopoles (26). The widely used dipolar spin-ice model (DSIM) (23) can be used to derive this magnetic monopoles in spin-ice (MMSI) picture. DSIM incorporates nearest-neighbor exchange interactions and long-range dipole interactions:

$$H_{DSI} = -J\sum_{<ij>} \boldsymbol{S}_i \cdot \boldsymbol{S}_j + Da^3 \sum_{i<j} \left(\frac{\boldsymbol{S}_i \cdot \boldsymbol{S}_j}{|\boldsymbol{r}_{ij}|^3} - \frac{3(\boldsymbol{S}_i \cdot \boldsymbol{r}_{ij})(\boldsymbol{S}_j \cdot \boldsymbol{r}_{ij})}{|\boldsymbol{r}_{ij}|^5} \right), \quad [5]$$

where a is the nearest-neighbor distance between moments, J is an exchange strength, and $D = \mu_0\mu^2/(4\pi a^3)$ is a nearest-neighbor dipole energy scale. This Hamiltonian is mathematically equivalent to a model where flips of the real Dy^{3+} dipoles are recast as two opposite magnetic charges which, through a sequence of spin flips, are hypothesized to form a fluid of delocalized magnetic monopoles (red and green in Fig. 2*C*) (26). At low temperatures these monopoles might then form a dilute neutral gas analogous to an electrolyte, so that a Debye–Hückel electrolyte model (27) suitably modified for magnetic monopoles may be used to describe a "magnetolyte" state (28). Such a fluid of delocalized magnetic monopole excitations, if extant, would constitute a highly novel magnetic state.

However, many observed properties of $Dy_2Ti_2O_7$ remain unexplained when they are analyzed using the DSIM/MMSI models. Although DSIM captures some of the diffuse neutron-scattering features of $Dy_2Ti_2O_7$, simulations based on Eq. **5** give an incomplete description of the data; additional exchange contributions from next-nearest and third-nearest neighbors are required to actually fit the measured scattering intensities precisely (29). Similarly, whereas the magnetic susceptibility $\chi(\omega,T) = \chi'(\omega,T) - i\chi''(\omega,T)$ is known empirically with high precision (30–33), no accurate quantitative model based on internally consistent parameterizations of $\chi'(\omega,T)$ and $\chi''(\omega,T)$ has been achieved using DSIM/MMSI (or any other) models. Moreover, the measured susceptibility of $Dy_2Ti_2O_7$ cannot be described by the simple Debye form (e.g., Eq. **2** with $\alpha = \gamma = 1$) that would be expected of a typical paramagnet (33). Microscopic approaches do not capture precisely the $Dy_2Ti_2O_7$ magnetization dynamics. For example, DSIM simulations do not accurately reproduce the measured $\chi(\omega,T)$ data at low temperatures (34). Furthermore, below ~0.5 K macroscopic relaxation rates in $Dy_2Ti_2O_7$ become ultraslow (20, 21, 30, 33, 35–37); this reflects a divergence of microscopic relaxation times (30, 33) that is unexplained quantitatively within the present DSIM/MMSI models. Thus, although Debye–Hückel calculations (28) and DSIM/MMSI simulations (38, 39) offer clear improvements over a simple Arrhenius form for $\tau(T)$, they still significantly underestimate the observed magnitude and rate of increase of τ below 1 K. In fact, as emphasized in a recent review (14), no studies of $Dy_2Ti_2O_7$ have yielded direct and unambiguous evidence of a fluid of delocalized magnetic monopoles. This motivates the search for a more accurate identification and understanding of the low-temperature magnetic state of this important compound.

Experimental Methods

To explore these issues, we introduce a novel boundary-free technique for studying magnetization transport in $Dy_2Ti_2O_7$. The innovation consists primarily of using a toroidal geometry for both the $Dy_2Ti_2O_7$ samples and the magnetization sensors, an arrangement with several important benefits. The first is that the superconducting toroidal solenoid (STS) can be used to both drive any magnetization flows azimuthally and to simultaneously and directly detect d***M***/dt throughout the whole torus. More significantly, this topology removes any boundaries in the direction of the magnetization transport. To achieve this sample topology, holes were pierced through disks of single-crystal $Dy_2Ti_2O_7$ (*SI Text*, section S1). A superconducting toroidal solenoid of CuNi-clad NbTi wire (diameter ~0.1 mm) is then wound around each $Dy_2Ti_2O_7$ torus (*SI Text*, section S1). Typical samples had an inner diameter ~2.5 mm, outer diameter ~6 mm, and thickness ~1 mm. The superconducting circuitry used to drive and measure d***M***/dt is shown schematically in Fig. 2*D*, along with indicators of the azimuthal $B\phi$ generated by the STS (blue arrows) and the putative flow of a mixed-sign monopole fluid (red/green arrows). The all-superconducting four-point I–V measurement circuit used to generate the $B\phi$-field and simultaneously measure the electromotive force (EMF) induced by d***M***/dt is shown schematically in Fig. 2*D*. These toroidal sample/coil assemblies were mounted on a dilution refrigerator and studied at temperatures 30 mK < T <3 K, and using currents not exceeding 30 mA in the STS ($B\phi$ < ~1 G, so always in the low-field limit $\mu B \ll k_B T$).

Time-Domain Measurements. Elementary magnetization dynamics experiments in the time domain are then carried out using the following repeated measurement cycle. First, a current (and thus $B\phi$) is switched on in the STS, and the EMF across this same coil V(t) is measured from when the switch-on transient ends until V(t) drops below our noise level. Next, the current (and $B\phi$) is turned off and we again measure the $V(t)$ response. The current is then turned on in the reverse direction ($-B\phi$) for the same time interval and turned off for the same time interval, and the procedure is repeated. Complete data sets for this sequence as a function of temperature are shown in *SI Text*, section S3.

Fig. 3*A* shows the time-dependent magnetization of $Dy_2Ti_2O_7$ determined from $V(t,T) \propto d\boldsymbol{M}/dt[t,T]$ at each temperature (Fig. 3*A*). To study these measurements in the context of KWW, we fit each transient $V(t,T)$ to the KWW function Eq. **3** and determine $\tau_{KWW}(T)$ and $\beta(T)$. The results are shown directly by plotting the measured $\log(V(t)/V_0)$ vs. $x(t) \equiv ((t)/\tau_{KWW}(T))^{\beta(T)}$ in Fig. 3*B*; for these temperatures $\beta \sim 0.75$. There we see that, for all measured

PHYSICS

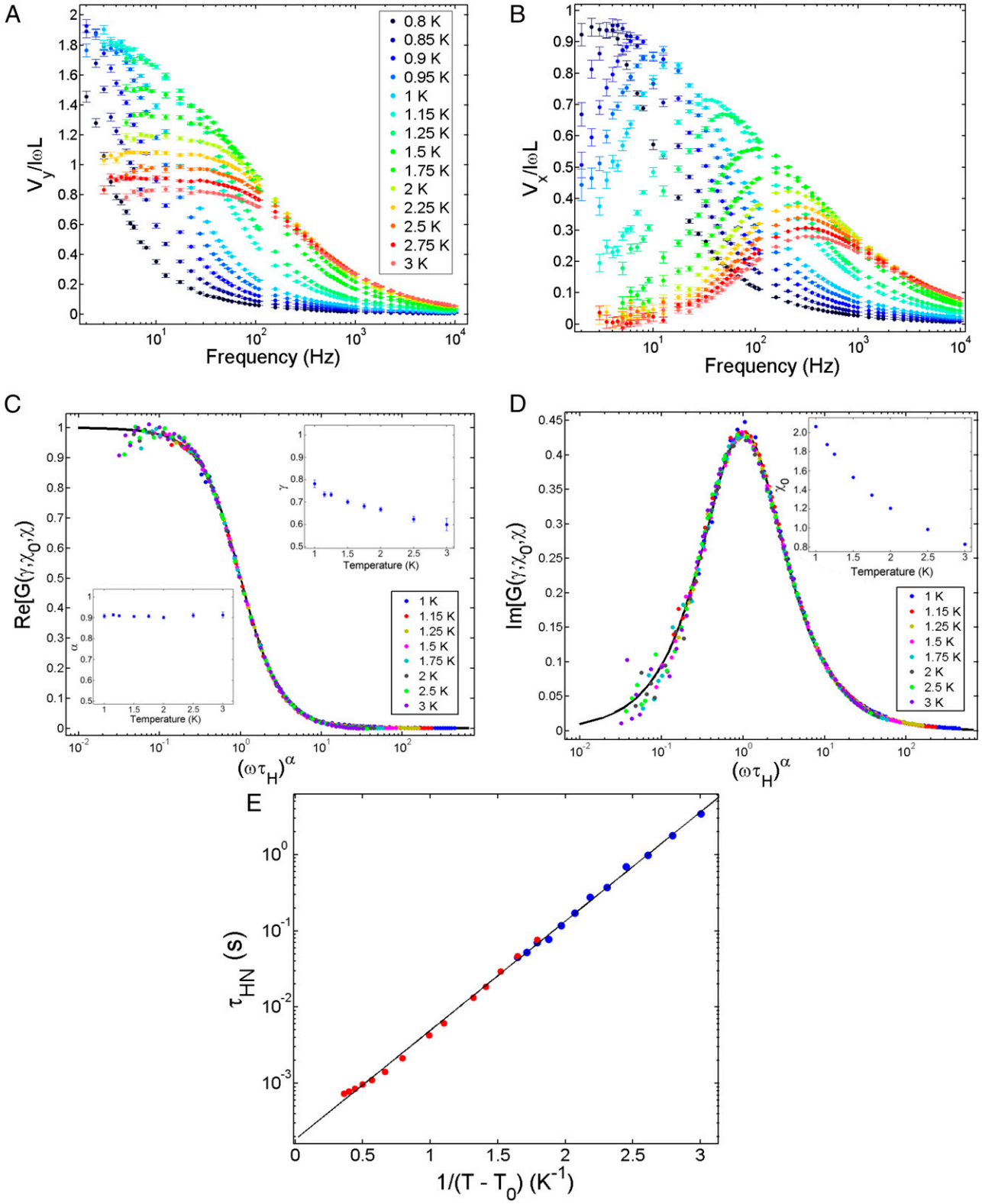

Fig. 4. HN magnetic susceptibility and VTF microscopic relaxation times. (*A*) Measured frequency and temperature dependence of the real component of the magnetic susceptibility calculated from the EMF component V_y that is 90° out of phase with the applied field. (*B*) Measured frequency and temperature dependence of the imaginary component of the magnetic susceptibility calculated from the EMF component V_x that is in phase with the applied field. (*C*) To demonstrate that the $Dy_2Ti_2O_7$ magnetic susceptibility $\chi(\omega, T)$ is comprehensively described by an HN form, we define in Eq. **8** a scaled susceptibility $G(\gamma, \chi)$ depending only upon γ, χ_0, and $\chi(\omega, T)$. Here, we plot $\mathrm{Re}[G(\gamma, \chi)]$ vs. $(\omega\tau)^{\alpha}$ for all our measured $\chi(\omega, T)$ showing a very high precision collapse of all our data to the HN form (shown as a solid line for $[\chi_0 = 1,\ \gamma = 1, \tau_{HN} = 1, \alpha = 0.91]$). (*Insets*) Fit values of $\gamma(T)$ and $\alpha(T)$. (*D*) $\mathrm{Im}[G(\gamma, \chi)]$ plotted vs. $(\omega\tau)^{\alpha}$ for all measured $\chi(\omega, T)$ again showing a high-precision collapse of all our data to the HN form (shown as a solid line for $[\chi_0 = 1,\ \gamma = 1, \tau_{HN} = 1, \alpha = 0.91]$) with identical parameters as in *A*. (*Inset*) Fit values of χ_0. (*E*) Measured microscopic relaxation times $\tau_{HN}(T)$ for magnetization in $Dy_2Ti_2O_7$ spanning the whole temperature range $0.575\ \mathrm{K} < T < 3\ \mathrm{K}$ plotted vs. $(T - T_o)^{-1}$ where $T_o = 242$ mK. This demonstrates clearly that magnetic relaxation in $Dy_2Ti_2O_7$ is governed by the VTF form (Eq. **1**) over almost four orders of magnitude in τ_{HN}.

transients over a range 600 mK < T < 900 mK, the $d\boldsymbol{M}/dt$ of $Dy_2Ti_2O_7$ is very well represented by a KWW time dependence. A complete set of all measured transients and KWW fits between 575 mK and 900 mK is shown in the *SI Text*. This puts the ultraslow magnetization dynamics in the same empirical class as classic supercooled liquids (1–4). Stretched-exponential relaxation has been previously seen in studies of single-crystal rods of $Dy_2Ti_2O_7$ (37) but there it was proposed that this relaxation occurred due to the open boundary conditions. However, our sample topology is a physical realization of periodic boundary conditions implying that our observed KWW relaxation is actually a fundamental property of the system.

Frequency-Domain Measurements. If KWW magnetization transient dynamics as in Fig. 3 are evidence for supercooling of a correlated magnetic fluid, the equivalent phenomena should also be observed as a universal HN form for the frequency-dependent complex magnetic susceptibility $\chi(\omega, T)$. To explore this possibility, we apply sinusoidal currents $I_0\cos(\omega t)$ to the STS and generate a field $B\phi\cos(\omega t+\phi)$ while simultaneously detecting the resulting EMF: $V(\omega, T) = V_x(\omega, T) + iV_y(\omega, T)$. Here, the $V(\omega, T)$ is due to temperature-dependent changes in the sample dynamical magnetization (*SI Text*, section S2). Directly from the experimental setup (*SI Text*, section S2) one can write $V_x(\omega, T) = -I_0\omega L\chi''$, $V_y(\omega, T) = -I_0\omega L\chi'$, where L is the effective geometrical inductance of the STS. A complete set of $\chi'(\omega, T)$ and $\chi''(\omega, T)$ measured in this fashion is shown in Fig. 4 *A* and *B* and described in *SI Text*, section S2. Equivalent phenomena were measured in three different $Dy_2Ti_2O_7$ tori ruling out any specific sample preparation or torus/coil geometry effects as the cause of reported phenomena. Empirically, the temperature and frequency dependence of the $\chi'(\omega, T)$ and $\chi''(\omega, T)$ in our studies is virtually identical to what has been reported previously. Until now, however, no quantitative internally consistent model for the susceptibility of $Dy_2Ti_2O_7$ has been identified. Here, we show that an HN form for a magnetic susceptibility

$$\chi_{HN}(\omega, T) = \chi_\infty + \frac{\chi_0}{(1+(i\omega\tau_{HN})^\alpha)^\gamma}, \qquad [6]$$

provides a comprehensive accurate internally consistent description for both $\chi'(\omega, T)$ and $\chi''(\omega, T)$ of $Dy_2Ti_2O_7$. To achieve this, we need to demonstrate that all our disparate $\chi(\omega, T)$ data (Fig. 4 *A* and *B*) have the same HN functional form. We define a scaled susceptibility $G(\gamma, \chi)$ that depends only upon γ, χ_0, and $\chi(\omega, T)$:

$$\begin{aligned}\mathrm{Re}[G(\gamma,\chi)] &\equiv \chi_0^{-(1/\gamma)}\left[(\chi')^2+(\chi'')^2\right]^{1/2\gamma}\cos\left[\frac{1}{\gamma}\arctan\left(\frac{\chi''}{\chi'}\right)\right]\\ \mathrm{Im}[G(\gamma,\chi)] &\equiv \chi_0^{-(1/\gamma)}\left[(\chi')^2+(\chi'')^2\right]^{1/2\gamma}\sin\left[\frac{1}{\gamma}\arctan\left(\frac{\chi''}{\chi'}\right)\right]\end{aligned}, \qquad [7]$$

where we have neglected χ_∞ because it is much smaller than χ_0 at our experimental temperatures (*SI Text*, section S2). As shown analytically in *SI Text*, section S2, if plotting $\mathrm{Re}[G(\gamma,\chi)]$ and $\mathrm{Im}[G(\gamma,\chi)]$ vs. $(\omega\tau)^\alpha$ collapses all $\chi(\omega, T)$ data onto a single curve, then the magnetic susceptibility exhibits a universal HN form. Fig. 4 *C* and *D* shows such a data collapse for $\chi(\omega, T)$ throughout our measured temperature range; the fine solid line is a plot of Eq. **7** using the susceptibility of Eq. **6** with $\chi_0 = \gamma = 1$. It is clear that $\chi_{HN}(\omega, T)$ fits the observed $Dy_2Ti_2O_7$ data precisely and comprehensively. To our knowledge, this is the first time that both $\chi'(\omega, T)$ and $\chi''(\omega, T)$ of $Dy_2Ti_2O_7$ have been quantitatively and simultaneously described by a single internally consistent function, across very wide frequency–temperature ranges and with Kramers–Kronig consistency. More importantly, because this HN form for magnetic susceptibility is functionally indistinguishable from the $\varepsilon(\omega, T)$ of supercooled liquids (1–3), it strongly implies supercooling of a correlated magnetic fluid in this compound.

Diverging Microscopic Relaxation Rates. A final test of the supercooled magnetic liquid hypothesis would be to show that the magnetic relaxation times diverge on a VTF trajectory for $Dy_2Ti_2O_7$. To determine microscopic relaxation times $\tau_0(T)$ spanning the whole temperature range, we used $\tau_{HN}(T)$ from fitting Eq. **6** simultaneously to $\chi'(\omega, T)$ and $\chi''(\omega, T)$ for 0.8 K < T < 3 K, and $\tau_{KWW}(T)$ from the time-domain $V(t,T)$ fitted by Eq. **3** and then converted to the equivalent $\tau_{HN}(T)$ for 0.58 K < T<0.85 K using Eq. **4**. As shown in Fig. 4*E*, the resulting $\tau_{HN}(T)$ of $Dy_2Ti_2O_7$ can, indeed, be represented by a VTF function (Eq. **1**) with high precision over many orders of magnitude ($T_0 \approx$ 0.24 K and fragility parameter $D \approx 14$). This unifies the evidence (Figs. 3 and 4) that the magnetic state of $Dy_2Ti_2O_7$ for 0.5 K < T < 3 K is a supercooled magnetic liquid.

Conclusions and Discussion

One may now reconsider the anomalous phenomena of $Dy_2Ti_2O_7$ in this new context. Empirically, our measured $\chi(\omega, T)$ data are in good agreement with earlier reports (30–33) implying that all can be describable by an HN susceptibility (Eq. **2**; Fig. 4 *A* and *B*). Also, whereas the Curie–Weiss temperature $T_{CW} \sim 1.2$ K (16) implies a tendency toward ferromagnetic order, no ordering is observed and, instead, a broad peak in specific heat $C(T)$ appears just below T_{CW} (18–22); this is as expected for a supercooled liquid (Fig. 1*A* and refs. 1–3). The location of Dy^{3+} moments in the highly anisotropic environment of the $Dy_2Ti_2O_7$ prevents ferromagnetic ordering at a temperature that might be expected from the nearest-neighbor interaction energy scale; this may be analogous to preventing the onset of a crystalline phase in glass-forming liquids due to anisotropic interactions between molecules. Moreover, ultraslow macroscopic equilibration is widely reported at lower temperatures (20, 35, 37) and is also just what one expects in a supercooled liquid approaching the glass transition (1–3). Our observed stretched-exponential form for ultraslow magnetization relaxation agrees well with previous studies (37). Although actually at odds with the predictions of DSIM/MMSI simulations for periodic geometries (39), this phenomenon is characteristic of a supercooled fluid (1–3). Finally, the published data on divergences of microscopic relaxation times (30, 33) are in good empirical agreement with ours, implying that the VTF form for $\tau(T)$ is general for $Dy_2Ti_2O_7$ (Eq. **1**; Fig. 4*E*). Thus, we conjecture that overall magnetization dynamics of $Dy_2Ti_2O_7$ are best explained if the system is a classical correlated-spin liquid that is supercooled and approaching a glass transition. Within this picture, the divergence temperature $T_0 \approx 240$ mK derived from our VTF fit (Fig. 4*E*) provides an estimate of the lowest temperature at which a metastable magnetic liquid state can survive under arbitrary cooling protocols; below this temperature we expect that $Dy_2Ti_2O_7$ must transition into either a heterogeneous glass phase or (with extremely slow cooling) a phase with global magnetic order.

To recapitulate: For the magnetic pyrochlore system $Dy_2Ti_2O_7$ we discover that the magnetic susceptibility $\chi(\omega, T)$ exhibits an HN form, the magnetic relaxation $\chi(t)$ simultaneously exhibits the KWW form, and the microscopic magnetic relaxation rates $\tau(T)$ occur on the VTF trajectory. When, in combination with a broad specific heat peak, this phenomenology is observed for the $\varepsilon(\omega, T)$ of a classic glass-forming material, it definitely identifies a supercooled liquid (1–3). Our observations therefore strongly imply that the magnetic state of $Dy_2Ti_2O_7$ is a supercooled classical spin liquid, approaching a glass transition. However, we emphasize that one should not expect any consequent magnetic glass to be a classic spin glass, because all of the $Dy_2Ti_2O_7$ spins are at ordered crystal lattice sites with locally identical spin Hamiltonians. And, indeed, $Dy_2Ti_2O_7$ is known to exhibit a very different field dependence from what is seen in classical spin glasses (30). The supercooled liquid characteristics of magnetization dynamics in $Dy_2Ti_2O_7$ (Figs. 3 and 4) more likely imply some form of persistent heterogeneous freezing in the microscopic configurations of strongly correlated spins (40, 41). Such a situation could also be described (somewhat redundantly) as freezing of monopole configurations. However, in terms of actual magnetization transport, the observed stretched-exponential time dependence of magnetization (Fig. 3; ref. 37) contradicts the predicted dynamics of both DSIM and MMSI models (39). Instead, one intriguing possibility is that the state of $Dy_2Ti_2O_7$ actually represents translationally invariant many-body localization of the spins (42–44). It will be fascinating, in this context, to reconsider the absence of magnetic ordering in other frustrated pyrochlores so as to determine if supercooled classical spin liquids occur therein.

ACKNOWLEDGMENTS. We are grateful to E. Fradkin, B. Gaulin, M. Gingras, S. Grigera, D. Hawthorn, R. Hill, E.-A. Kim, J. Kycia, M. J. Lawler, A. P. Mackenzie,

R. Melko, and J. Sethna for very helpful discussions and communications. This research is funded by the Gordon and Betty Moore Foundation's Emergent Phenomena in Quantum Systems Initiative through Grant GBMF4544 and by the Engineering and Physical Sciences Research Council Programme Grant "Topological Protection and Non-Equilibrium States in Correlated Electron Systems."

1. Ediger M, Angell C, Nagel S (1996) Supercooled liquids and glasses. *J Phys Chem* 100(31):13200–13212.
2. Tarjus G, Kivelson S, Nussinov Z, Viot P (2005) The frustration-based approach of supercooled liquids and the glass transition: A review and critical assessment. *J Phys Condens Matter* 17(50):R1143–R1182.
3. Cavagna A (2009) Supercooled liquids for pedestrians. *Phys Rep* 476(4-6):51–124.
4. Bohmer R, Ngai K, Angell C, Plazek D (1993) Nonexponential relaxations in strong and fragile glass formers. *J Chem Phys* 99(5):4201–4209.
5. Havriliak S, Negami S (1967) A complex plane representation of dielectric and mechanical relaxation processes in some polymers. *Polymer (Guildf)* 8:161–210.
6. Havriliak S, Jr, Havriliak S (1994) Results from an unbiased analysis of nearly 1000 sets of relaxation data. *J Non-Cryst Solids* 172-174:297–310.
7. Kohlrausch R (1854) Theorie des elektrischen ruckstandes in der leidner flasche. *Ann Phys Chemie (Poggendorff)* 91:179–213.
8. Alvarez F, Alegra A, Colmenero J (1991) Relationship between the time-domain Kohlrausch-Williams-Watts and frequency-domain Havriliak-Negami relaxation functions. *Phys Rev B Condens Matter* 44(14):7306–7312.
9. Harris M, Bramwell S, Holdsworth P, Champion J (1998) Liquid-gas critical behavior in a frustrated pyrochlore ferromagnet. *Phys Rev Lett* 81(20):4496–4499.
10. Lacroix C, Mendels P, Mila F, eds (2011) *Introduction to Frustrated Magnetism: Materials, Experiments, Theory*, Springer Series in Solid-State Sciences (Springer, Heidelberg).
11. Gardner J, Gingras M, Greedan E (2010) Magnetic pyrochlore oxides. *Rev Mod Phys* 82(1):53–107.
12. Balents L (2010) Spin liquids in frustrated magnets. *Nature* 464(7286):199–208.
13. Castelnovo C, Moessner R, Sondhi S (2012) Spin ice, fractionalization, and topological order. *Annu Rev Condens Matter Phys* 3:35–55.
14. Gingras MJ, McClarty PA (2014) Quantum spin ice: A search for gapless quantum spin liquids in pyrochlore magnets. *Rep Prog Phys* 77(5):056501.
15. Rosenkranz S, et al. (2000) Crystal-field interaction in the pyrochlore magnet Ho2-Ti2O7. *J Appl Phys* 87(9):5914–5916.
16. Fukazawa H, Melko R, Higashinaka R, Maeno Y, Gingras M (2002) Magnetic anisotropy of the spin-ice compound $Dy_2Ti_2O_7$. *Phys Rev B* 65(5):054410.
17. Dunsiger SR, et al. (2011) Spin ice: Magnetic excitations without monopole signatures using muon spin rotation. *Phys Rev Lett* 107(20):207207.
18. Klemke B, et al. (2011) Thermal relaxation and heat transport in the spin ice material $Dy_2Ti_2O_7$. *J Low-Temp Phys* 163(5-6):345–369.
19. Higashinaka R, Fukazawa H, Yanagishima D, Maeno Y (2002) Specific heat of $Dy_2Ti_2O_7$ in magnetic fields: Comparison between single-crytalline and polycrystalline data. *J Phys Chem Solids* 63(6-8):1043–1046.
20. Pomaranski D, et al. (2013) Absence of Pauling's residual entropy in thermally equilibrated $Dy_2Ti_2O_7$. *Nat Phys* 9:353–356.
21. Ramirez A, Hayashi A, Cava R, Siddharthan R (1999) Zero-point entropy in "spin ice." *Nature* 399:333–335.
22. Morris DJ, et al. (2009) Dirac strings and magnetic monopoles in the spin ice $Dy_2Ti_2O_7$. *Science* 326(5951):411–414.
23. Gingras MJ, den Hertog BC (2000) Dipolar interactions and origin of spin ice in Ising pyrochlore magnets. *Phys Rev Lett* 84(15):3430–3433.
24. Bramwell ST, Gingras MJ (2001) Spin ice state in frustrated magnetic pyrochlore materials. *Science* 294(5546):1495–1501.
25. Melko R, Gingras M (2004) Monte Carlo studies of the dipolar spin ice model. *J Phys Condens Matter* 16(43):R1277–R1319.
26. Castelnovo C, Moessner R, Sondhi SL (2008) Magnetic monopoles in spin ice. *Nature* 451(7174):42–45.
27. Levin Y (2002) Electrostatic correlations: From plasma to biology. *Rep Prog Phys* 65(11):1577–1632.
28. Castelnovo C, Moessner R, Sondhi S (2011) Debye-Hückel theory for spin ice at low temperature. *Phys Rev B* 84(14):144435.
29. Yavors'kii T, Fennell T, Gingras MJ, Bramwell ST (2008) $Dy_2Ti_2O_7$ spin ice: A test case for emergent clusters in a frustrated magnet. *Phys Rev Lett* 101(3):037204.
30. Snyder J, et al. (2004) Low-temperature spin freezing in the $Dy_2Ti_2O_7$ spin ice. *Phys Rev B* 69(6):064414.
31. Matsuhira K, et al. (2011) Spin dynamics at very low temperature in spin ice $Dy_2Ti_2O_7$. *J Phys Soc Jpn* 80(9):123711.
32. Bovo L, Bloxsom JA, Prabhakaran D, Aeppli G, Bramwell ST (2013) Brownian motion and quantum dynamics of magnetic monopoles in spin ice. *Nat Commun* 4:1535–1542.
33. Yaraskavitch L, et al. (2012) Spin dynamics in the frozen state of the dipolar spin ice $Dy_2Ti_2O_7$. *Phys Rev B* 85(2):020410.
34. Takatsu H, et al. (2013) AC susceptibility of the dipolar spin ice $Dy_2Ti_2O_7$: Experiments and Monte Carlo simulations. *J Phys Soc Jpn* 82(10):104710.
35. Giblin S, Bramwell S, Holdsworth P, Prabhakaran D, Terry I (2011) Creation and measurement of long-lived magnetic monopole currents in spin ice. *Nat Phys* 7:252–258.
36. Orendáć M, et al. (2007) Magnetocaloric study of spin relaxation in dipolar spin ice $Dy_2Ti_2O_7$. *Phys Rev B* 75(10):104425.
37. Revell H, et al. (2012) Evidence of impurity and boundary effects on magnetic monopole dynamics in spin ice. *Nat Phys* 9:34–37.
38. Jaubert L, Holdsworth P (2009) Signature of magnetic monopole and Dirac string dynamics in spin ice. *Nat Phys* 5:258–261.
39. Jaubert LD, Holdsworth PC (2011) Magnetic monopole dynamics in spin ice. *J Phys Condens Matter* 23(16):164222.
40. Cépas O, Canals B (2012) Heterogeneous freezing in a geometrically frustrated spin model without disorder: Spontaneous generation of two timescales. *Phys Rev B* 86(2): 024434.
41. Nussinov Z, Batista CD, Normand B, Trugman SA (2007) High-dimensional fractionalization and spinon deconfinement in pyrochlore antiferromagnets. *Phys Rev B* 75(9):094411.
42. De Roeck W, Huveneers F (2014) Scenario for delocalization in translation-invariant systems. *Phys Rev B* 90(16):165137.
43. Yao N, Laumann C, Cirac J, Lukin M, Moore J (2014) Quasi many-body localization in translation-invariant systems. arXiv:1410.7407.
44. Schiulaz M, Silva A, Muller M (2015) Dynamics in many-body localized quantum systems without disorder. *Phys Rev B* 91(18):184202.